BIOCHEMISTRY
including biophysical chemistry & molecular biology

Article

pubs.acs.org/biochemistry

His86 from the N-Terminus of Frataxin Coordinates Iron and Is Required for Fe−S Cluster Synthesis

Leslie E. Gentry, Matthew A. Thacker, Reece Doughty,[‡] Russell Timkovich, and Laura S. Busenlehner*

Department of Chemistry, The University of Alabama, Tuscaloosa, Alabama 35487-0336, United States

Supporting Information

ABSTRACT: Human frataxin has a vital role in the biosynthesis of iron−sulfur (Fe−S) clusters in mitochondria, and its deficiency causes the neurodegenerative disease Friedreich's ataxia. Proposed functions for frataxin in the Fe−S pathway include iron donation to the Fe−S cluster machinery and regulation of cysteine desulfurase activity to control the rate of Fe−S production, although further molecular detail is required to distinguish these two possibilities. It is well established that frataxin can coordinate iron using glutamate and aspartate side chains on the protein surface; however, in this work we identify a new iron coordinating residue in the N-terminus of human frataxin using complementary spectroscopic and structural approaches. Further, we demonstrate that His86 in this N-terminal region is required for high affinity iron coordination and iron assembly of Fe−S clusters by ISCU as part of the Fe−S cluster biosynthetic complex. If a binding site that includes His86 is important for Fe−S cluster synthesis as part of its chaperone function, this raises the possibility that either iron binding at the acidic surface of frataxin may be spurious or that it is required for protein−protein interactions with the Fe−S biosynthetic quaternary complex. Our data suggest that iron coordination to frataxin may be significant to the Fe−S cluster biosynthesis pathway in mitochondria.

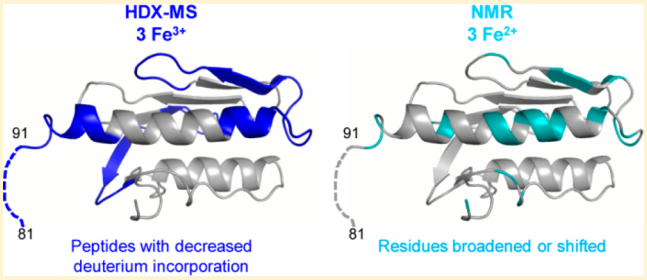

Many neurodegenerative diseases are linked to imbalances in metal homeostasis. The autosomal recessive neuromuscular disorder Friedreich's ataxia (FA) is one such example. FA is primarily caused by a $(GAA)_n$ triplet repeat expansion in the first intron of the frataxin gene.[1] This results in decreased transcription and/or translation of the gene and, therefore, significantly reduced levels of frataxin in mitochondria of the heart, spinal cord, and other tissues. FA is characterized by a marked increase in mitochondrial iron, oxidative stress, decreased activities of enzymes with iron−sulfur clusters (Fe−S), and electron transport chain dysfunction. Cells from FA patients indicate cytosolic iron deficiency even though iron levels are highly elevated in mitochondria.[2]

The function of frataxin has been debated since it was first linked to FA in 1996. By far, the most convincing role is one in Fe−S cluster biosynthesis. Heart biopsies of FA patients reveal decreased activities of Fe−S enzymes in the electron transport chain and in the tricarboxylic acid cycle. The same enzyme deficiencies were observed in *Saccharomyces cerevisiae* strains deficient in Yfh1, the frataxin homologue in yeast, and in other model systems.[3] It is apparent that, in some way, frataxin deficiency disrupts production of Fe−S clusters. Fe−S clusters are assembled in the mitochondria of eukaryotic cells via the ternary Fe−S cluster biosynthetic complex, which consists of the cysteine desulfurase NFS1, the Fe−S scaffold protein ISCU, and the accessory protein ISD11.[4] Frataxin physically and functionally interacts with ISCU, NFS1, and ISD11; therefore, it is suggested to be a member of the Fe−S complex.[5] Some research suggests that frataxin is an iron-chaperone that delivers Fe^{2+} to the Fe−S cluster complex.[6] *In vitro*, frataxin stimulates the rate of formation of [2Fe-2S] clusters on the surface of ISCU with externally supplied sulfide[7] and photoactivated chemical cross-linking[8] confirms the interaction between frataxin and ISCU. Other studies indicate that frataxin may regulate Fe−S cluster synthesis through its stimulation of NFS1 cysteine desulfurase activity as part of the ISCU/NFS1/ISD11 complex.[9,10] For either case, iron is delivered directly or indirectly through NSF1 activation to the ternary ISCU/NFS1/ISD11 Fe−S machinery for cluster synthesis.

The structures of monomeric apo-frataxin have been solved for the human, yeast, and bacterial homologues, revealing a unique and conserved fold.[11] One striking feature of all frataxin homologues is a clustering of negatively charged aspartate and glutamate residues on one surface of the protein called the "acidic ridge". NMR studies indicated metal binding at or near these residues in the human,[12,13] yeast,[14,15] and bacterial frataxin homologues.[13] The three-dimensional structures of various frataxin proteins have provided much needed structural information, but there is still ambiguity in the coordination environment since there is no structure with iron bound. There is also uncertainty with respect to the Fe^{2+} stoichiometry. Part of the ambiguity lies in the ability of frataxin to coordinate most divalent metal ions using the acidic residues on the surface.[16]

Received: April 8, 2013
Revised: July 29, 2013
Published: August 2, 2013

   dx.doi.org/10.1021/bi400443n | *Biochemistry* 2013, 52, 6085−6096

Additionally, reducing agents and some buffers also chelate metal ions, and many frataxin studies employed these competitors in excess over the frataxin concentration to keep iron in a reduced state. Thus, the stoichiometries and measured dissociation constants could be affected by these chemical components. From various experiments, it appears that human frataxin contains 1−2 Fe^{2+} binding sites with nanomolar to micromolar dissociation constants.[17] The locations of the actual binding sites are assumed to be along the acidic ridge and into the β1-strand, based on NMR iron titrations of frataxin.[13,14,18] However, mutation of specific aspartate and glutamate residues within the acidic ridge affect frataxin binding with ISCU, the scaffold for Fe−S cluster synthesis, but does not change the total number of Fe^{2+} binding sites.[9] This may indicate that metal binding at the acidic ridge is superfluous and that there may be additional, specific Fe^{2+} binding sites that are not readily identifiable by current techniques.

Despite many years of research, there are still three main questions about frataxin iron binding: (1) what is the stoichiometry of Fe^{2+} binding to human frataxin?; (2) what residues are involved in coordination?; and (3) which of these Fe^{2+} sites are functionally relevant for Fe−S cluster formation by ISCU? To address these questions, we characterized the metal coordination environment and stoichiometries using Fe^{2+}, Fe^{3+}, and Co^{2+}, which are common surrogates to probe Fe^{2+} sites in proteins because they have characteristic electronic absorptions based on their environment and are not sensitive to aerobic conditions.[19] These properties make Co^{2+} and Fe^{3+} amenable to UV−visible and NMR spectroscopies. Since conformational or dynamics changes in frataxin should accompany metal binding, backbone amide hydrogen/deuterium exchange mass spectrometry (HDX−MS) was used to characterize structural perturbations in solution. Herein, we report that frataxin binds ∼3 metal ions and that one of these binding sites uses a previously unknown residue (His86) from the disordered N-terminal tail, which is functionally required for Fe^{2+} delivery to ISCU for Fe−S synthesis *in vitro*.

EXPERIMENTAL PROCEDURES

Materials. ACS-grade HEPES, dioxane-free IPTG, HPLC grade water, and HPLC grade acetonitrile were obtained from EMD Millipore (Billerica, MA). Deuterium oxide (99.99% at. D), ACS-grade Bis-Tris, and ferrozine were from Acros Organics (Morris Plains, NJ). Ultrapure magnesium chloride and ferric chloride were by Fisher Chemical (Fairlawn, NJ). Deuterated d_{18}-HEPES and ^{15}N-ammonium sulfate were obtained from Cambridge Isotopes (Andover, MA). Other reagents included porcine pepsin (3200−4500 units/mg) from Sigma-Aldrich (St. Louis, MO), HPLC grade 2-propanol from Honeywell (Franklin, PA), cobaltous chloride from Macron Chemicals (Center Valley, PA), ferrous ammonium sulfate from MP Biomedical (Santa Ana, CA), and EDTA from BDH Merck (Radnor, PA).

Purification of Human Frataxin. Human frataxin corresponding to residues 81−210, or the mature form, was expressed in *Escherichia coli* BL21(DE3)*pLysS* from *pET81−210Fxn*, as described.[8] Purification was performed in the presence of 2 mM EDTA in Chelex-treated, metal-free water. All glassware was rinsed with 10% nitric acid and metal-free water to remove trace metals. Frataxin concentrations were determined spectroscopically using $\varepsilon_{280\ nm}$ = 26.93 mM^{-1} cm^{-1}. The amount of zinc and iron in purified frataxin was determined via an AAnalyst 400 atomic absorption spectrometer (Perkin-Elmer, Waltham, MA) and was negligible.

UV−Visible Titrations. Titrations were performed on an Agilent 8453 spectrophotometer (Santa Clara, CA). For cobalt titrations, 300−400 μM frataxin in Chelex-treated 50 mM HEPES (pH 7.4), 400 mM NaCl, and 5% glycerol was titrated with a cobalt chloride stock solution in the same buffer. Co^{2+} was added in 5−10 μL increments, incubated for 5 min at 23 °C, and UV−visible spectra were collected from 200−800 nm. Each spectrum was corrected for dilution.

Colorimetric Fe^{2+} titrations required ferrozine, a Fe^{2+} specific chelator. All solutions were degassed and prepared in a Vacuum Atmosphere anaerobic glovebox. A 0.53 M stock of Fe^{2+} was made in 25 mM HEPES (pH 7.4), 150 mM NaCl. A 6.5 mM ferrozine stock was prepared in the same buffer with 2.5 M ammonium acetate. Samples of 108 μM with and without 13 μM apo-frataxin were made with increasing Fe^{2+} concentrations and spectra were collected from 240−800 nm. The Fe^{2+}−ferrozine$_3$ complex has a molar extinction at 562 nm of 27.9 mM^{-1} cm^{-1} and a formation constant (K_f) of 3.65 × 10^{15} M^{-3}.[20]

Fluorescence Titrations. Intrinsic tryptophan fluorescence titrations were performed at 23 °C using a Spex Fluoromax-3 fluorimeter (Edison, NJ) with ∼5 μM frataxin in either 50 mM HEPES (pH 7.4), 400 mM NaCl, 5% glycerol (Co^{2+} titrations), or 50 mM Bis-Tris (pH 7.4), 400 mM NaCl, and 5% glycerol (Fe^{3+} titrations) using an excitation wavelength of 295 nm. The metal titrant concentrations were determined by atomic absorption. After each addition of metal, the sample was equilibrated for 3 min with stirring at 23 °C. Fluorescence emission spectra were collected from 270−450 nm and corrected for dilution. Since the addition of Fe^{3+} leads to increased absorbance in this region of the spectrum, the fluorescence data were corrected for inner filter effect with an equivalent UV−vis titration of frataxin under the same conditions. This procedure was repeated with Co^{2+} for experimental continuity. The corrected fluorescence intensity was determined using eq 1.[21]

$$F_{corrected} = F_i \times 10^{\left(\frac{Abs_{295nm} + Abs_{343nm}}{2}\right)} \quad (1)$$

The initial fluorescence intensity (F_0) at the emission maximum wavelength was subtracted from each titration point ($F_i - F_0$), which was plotted against total metal concentration. The binding curves are stoichiometric (i.e., no "free" metal exists during the titration); therefore, the equilibrium binding constants obtained from fitting are not representative of the true K_d values and are not reported.[21]

Nuclear Magnetic Resonance Spectroscopy. One liter of M9 minimal media supplemented with 1 g/L 86% ^{15}N-ammonium sulfate was inoculated, as described, and grown at 37 °C to OD_{600} = 0.8, and then induced with 1 mM IPTG for 4 h. Cells were harvested at OD_{600} 1.8−2.0 and purified as described except the final buffer was Chelex-treated 25 mM HEPES-d_{18} (pH 7.0) with 100 mM NaCl. MALDI−TOF mass spectrometry confirmed ∼85% ^{15}N-enrichment in the purified NMR sample. Co^{2+}, Mg^{2+}, and Fe^{2+} titrant stocks were made in the HEPES-d_{18} buffer at pH 7.0, and their concentrations were determined by atomic absorption.

^{1}H−^{15}N HSQC spectra were collected for 0.56 mM apo-^{15}N-frataxin with 5% (v/v) D_2O. Resonances were assigned according to ref 22. Titrations from 0.2−6.0 mol equiv of

Co^{2+} and Mg^{2+} were performed aerobically. Individual NMR samples containing 1.0−4.0 mol equiv of Fe^{2+} were prepared anaerobically. NMR data were collected at 298 K on a Brüker Avance 600 MHz spectrometer (Fremont, CA) with a triple resonance $^{1}H/^{13}C/^{15}N$ probe equipped with *z*-axis pulsed field gradients. The fingerprint main chain amide region was recorded by the two-dimensional $^{1}H-^{15}N$-HSQC experiment[23] using the standard Brüker pulse program. Data collection time per spectrum ranged from 1.5 to 20 h to improve signal-to-noise ratios. Data were processed using NMRPipe[24] and SPARKY (T. D. Goddard and D. G. Kneller, University of California, San Francisco). The data matrix consisted of 2048 points in the proton dimension centered on the water resonance and 128 points in the nitrogen dimension centered at 117 ppm. Data in both dimensions were apodized with a shifted squared sine bell function and zero-filled prior to Fourier transformation. After transformation, data in both directions were baseline corrected with the default polynomial function of NMRPipe. Normalized amide chemical shifts (δ_{NH}) were calculated using the change in chemical shift from apo-frataxin values of the ^{1}H (δ_H) and ^{15}N (δ_N) resonances upon each addition of metal as shown in eq 2, modified from ref 25.

$$\delta_{NH} = \sqrt{(\delta_H)^2 + \left(\frac{\delta_N}{5}\right)^2} \quad (2)$$

Amide Hydrogen/Deuterium Exchange Mass Spectrometry. Twenty micrograms of frataxin was added to 100 μL of 0.1 M potassium phosphate (pH 2.3) containing 20 μg of pepsin. After a 5 min digestion on ice, the sample was separated on a 1 mm × 50 mm C18 column (Phenomenex, Torrence, CA) equilibrated at 0.1 mL/min by a ThermoFinnigan Surveyor HPLC connected to a TSQ Quantum mass spectrometer (San Jose, CA). Peptides were eluted with a 2%−50% acetonitrile gradient in water with 0.4% formic acid over 20 min and subjected to data-dependent tandem MS/MS collision-induced dissociation in positive-ion mode. Peptide assignments were made through Protein Prospector (http://prospector.ucsf.edu/) and Peaks.[26] The complete map is shown in Figure 1.

The aerobic HDX reactions were performed in triplicate with frataxin containing 0, 1, 2, and 3 mol equiv of either Co^{2+} or Fe^{3+}. Deuterium exchange reactions in 0.2 mL thin-walled tubes containing 5 μL of 580 μM frataxin (30 μM) were initiated with 45 μL of deuterium oxide (99.99% at. D_2O). Samples were incubated at 23 °C between 15 s−6 h. Exchange was quenched with 50 μL of 0.1 M potassium phosphate (pH 2.3; 0 °C) and placed on ice. After 10 s, 2 μL of 20 μg/μL pepsin was added and incubated 5 min at 0 °C. For HDX with reduced Fe^{2+}, we performed all steps in an anaerobic glovebox (<0.1 ppm O_2) using highly degassed stock solutions. Iron was prepared fresh (from solid) inside the glovebox, and the concentration of reduced Fe^{2+} was measured anaerobically with a bathophenanthrolinedisulfonate (BPS) colorimetric assay. The total concentration of iron was determined by atomic absorption. Our Fe^{2+} stocks contained <5% of contaminating Fe^{3+}. Deuterium exchange reactions in 0.2 mL thin-walled tubes containing 5 μL of 580 μM frataxin (30 μM) with 1, 2, 3, and 4 equiv of Fe^{2+} were initiated with 45 μL of deuterium oxide (99.99% at. D_2O). Samples were immediately sealed with parafilm and removed from the glovebox. Addition of quench solution and pepsin digestion was as above. The exposure to air upon addition of acidic quench is appropriate since the exchange reaction will have essentially stopped. As a control test for iron oxidation, mock samples of Fe^{2+}-frataxin in H_2O were incubated for 15 min, returned to the glovebox for BPS analysis, which revealed, on average, that 16% Fe^{3+} was present. Additional, longer incubations were not performed.

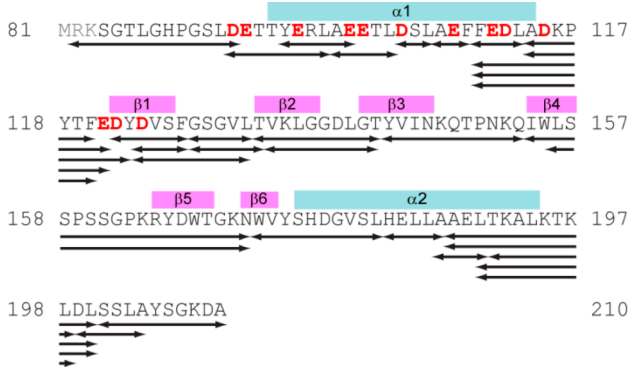

Figure 1. Identified peptides from pepsin digestion of frataxin. Frataxin (residues 81−210) was digested with pepsin and subjected to tandem mass spectrometry. Peptide amino acid sequences are indicated with arrows. The secondary structure as determined from PDB: 1LY7 is indicated, where α-helices are in light blue and β-strands are in pink. Residues in red are acidic residues from α1 and β1.[12]

Pepsin-generated peptides were separated by HPLC, as described, except that the solvent bottles, injector, and column were submerged in an ice bath, and the elution was 2%−35% acetonitrile over 10 min. Mass spectra were recorded using positive-ion electrospray ionization with a capillary temperature of 190 °C and a spray voltage of 3.5 kV. A control to account for natural isotope abundance (m_0) was prepared as other samples except that H_2O was used instead of D_2O.[27] Another control to correct for deuterium loss during chromatography (m_{100}) required frataxin to be completely exchanged for deuterium (m_{100}). This was done by incubating 5 μL of 580 μM frataxin with 45 μL of D_2O for at least 5 h at 60 °C.[27] The sample was then quenched and digested, as described. Deuterium loss during HPLC varied from 18−36%. HDX−MS data were averaged and processed by HDExaminer (Sierra Analytics, Modesto, CA). The percent deuterium incorporation (%*D*) was calculated using eq 3

$$\%D = \left(\frac{m_t - m_0}{m_{100} - m_0}\right) \times 100 \quad (3)$$

where m_t is the centroid value of the peptide at time *t*, m_0 is the nondeuterated peptide, and m_{100} is the fully deuterated peptide.[27] The percentage of deuterium incorporated was plotted and fit to single-, double-, or triple-exponential equations to give the percentage of amide protons exchanging for deuterons ($\%D_n$) at a given rate constant (k_n).[28] Amides that exchange faster than $k_n \geq 4$ min^{-1} are considered the fast phase. Those that have rate constants slower than $k_n = 1 \times 10^{-5}$ min^{-1} are considered "non-exchangeable" under our experimental conditions.

Mutagenesis of H86A in Frataxin. The codon for His86 in *pET81−210Fxn* was mutated to Ala via site-directed mutagenesis using QuikChange Lightning (Agilent, Santa Clara, CA). H86A frataxin was expressed in BL21(DE3)*pLysS* and purified as for the wild-type protein.[8] Co^{2+} and Fe^{3+} titrations monitored by UV−visible spectroscopy of H86A

dx.doi.org/10.1021/bi400443n | *Biochemistry* 2013, 52, 6085−6096

frataxin were performed as for wild-type. The Fe^{2+} titration of H86A frataxin in the presence of ferrozine chelator was also as described for the wild-type frataxin protein.

Purification of D37A ISCU. The *pET-mISCU* plasmid[29] was graciously obtained from Dr. Tracey Rouault (National Institutes of Health, Bethesda, MD). The codon for Asp37 was mutated to that for Ala, and a stop codon was introduced after the codon for Lys133 using QuikChange mutagenesis (Agilent, Santa Clara, CA). D37A ISCU was expressed in BL21(DE3) *pLysS* and purified as described for native ISCU.[8] D37A ISCU samples were anaerobically dialyzed into Chelex-treated 50 mM HEPES (pH 7.4), 150 mM NaCl with 10% glycerol. The concentration of ISCU was determined spectroscopically using $\varepsilon_{280\ nm}$ = 9.97 mM^{-1} cm^{-1}.

Fe−S Cluster Assembly Assays. All reactions were performed in an anaerobic cuvette fitted with a gastight syringe before removal from the glovebox. The reaction buffer was 25 mM HEPES (pH 7.4) with 150 mM NaCl. Frataxin or H86A frataxin (100 μM) was incubated with 200 μM ferrous ammonium sulfate (2 Fe^{2+}:1 frataxin) for 30 min at 25 °C. The reaction containing 100 μM D37A ISCU and 2.4 mM sodium sulfide was initiated by frataxin with 2 equiv of Fe^{2+} and was monitored at 426 nm using an Agilent 8453 spectrophotometer (Santa Clara, CA) in kinetics mode.[7] Controls included D37A ISCU with 200 μM ferrous ammonium sulfate (no frataxin), as well as with 200 μM Fe^{2+} bound to bovine serum albumin (BSA). The data were fit to a first-order rate equation (eq 4) to determine the initial rate of Fe−S cluster assembly,

$$\text{rate} = A_1 e^{-k_1 t} \quad (4)$$

where A_1 is the amplitude of the first-order rate, k_1, as a function of time, t.

RESULTS

Metal Coordination Environment and Stoichiometry. Mature human frataxin (residues 81−210) lacks cysteine residues, and therefore the Fe^{2+}−frataxin complex does not have electronic transitions within the visible range.[30] Experiments with ferrous iron require rigorous anaerobic or reducing conditions. Because many reducing agents can coordinate metals and exhibit metal-based absorptions, they should be excluded in binding experiments.[31] However, Co^{2+} is a common surrogate to aerobically probe Fe^{2+} binding sites in proteins and has electronic absorptions in the UV−visible region.[19] The Co^{2+} titration of frataxin reveals broad, overlapping transitions centered at 532 and 485 nm after 1 equiv of Co^{2+}, which is consistent with oxygen and/or nitrogen-coordination.[32] As additional Co^{2+} binds to frataxin, there is a blue shift to 511 and 466 nm, which could indicate more oxygen-based coordination.[33] The low molar absorptivities for the Co^{2+} d−d transitions (ε < 15 M^{-1} cm^{-1}) indicate octahedral geometry.[32] The Co^{2+} binding isotherm for frataxin is more linear in shape than hyperbolic, which is characteristic for stoichiometric binding, so ∼3 Co^{2+} binding sites were estimated (Figure 2). To further confirm the stoichiometry, metal titrations of frataxin, which contains three tryptophan residues, were followed by intrinsic tryptophan fluorescence. The emission (λ_{max} at 343 nm) is quenched by Co^{2+} and saturates at ∼3 equiv (Figure 3A), consistent with UV−visible titrations. Frataxin was also titrated with Fe^{3+} and displayed saturation after ∼3 mol equiv of Fe^{3+} (Figure 3B).

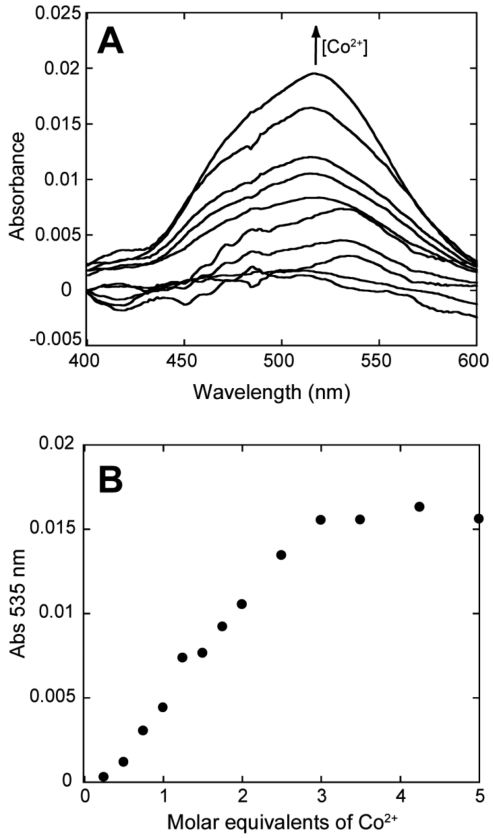

Figure 2. UV−visible cobalt titration of frataxin. (A) Shown are representative spectra from a Co^{2+} titration of 300 μM frataxin. Broad *d-d* transitions from 450−550 nm are observed with a λ_{max} of 535 nm. (B) The isotherm indicates saturation at ∼3 equiv of Co^{2+} per frataxin protein.

To estimate apparent affinities for ferrous iron, samples containing the Fe^{2+}-specific colorimetric chelator ferrozine, with and without frataxin, were incubated with increasing concentrations of Fe^{2+} (Figure 4). The Fe^{2+}−ferrozine$_3$ (1:3) complex absorbs at 562 nm (ε_{562} = 27.9 mM^{-1} cm^{-1}) with an apparent K_f of 10^{15} M^{-3}.[20] The sample containing frataxin clearly binds 1 equiv of Fe^{2+} before the purple color of Fe^{2+}−ferrozine$_3$ forms (Figure 4). This indicates that frataxin possesses one Fe^{2+} site of higher affinity than ferrozine, but the remaining two sites are of lower affinity than ferrozine.

HSQC NMR Co^{2+} and Fe^{2+} Titrations. To gain more insight into the localization of the surrogate metal compared to the native metal, $^1H-^{15}N$ HSQC spectra were collected from uniformly ^{15}N-labeled apo−frataxin titrated with Co^{2+} (aerobic) and with Fe^{2+} (anaerobic). Residues 81−90 were not observed due to intrinsic disorder.[22] Co^{2+} and Fe^{2+} are paramagnetic so through-bond coupling of the metal's free electrons and protein nuclei lead to large chemical shifts for amide nitrogens and protons near a bound metal, as well as line broadening of nuclei in close proximity.[34] It is assumed that $MgCl_2$, which is often used to reduce adventitious metal binding, could be included in Co^{2+} and Fe^{2+} titrations because diamagnetic metals like Mg^{2+} do not strongly affect chemical shifts.

Aerobic Co^{2+} binding to frataxin with and without 10 mM Mg^{2+} was investigated to assess its ability to alleviate nonspecific metal binding. It is observed that inclusion of 10 mM Mg^{2+} alters Co^{2+} binding isotherms for several residues within $\alpha1/\beta1$ (Figure S1, Supporting Information). Thus, all

dx.doi.org/10.1021/bi400443n | *Biochemistry* 2013, 52, 6085−6096

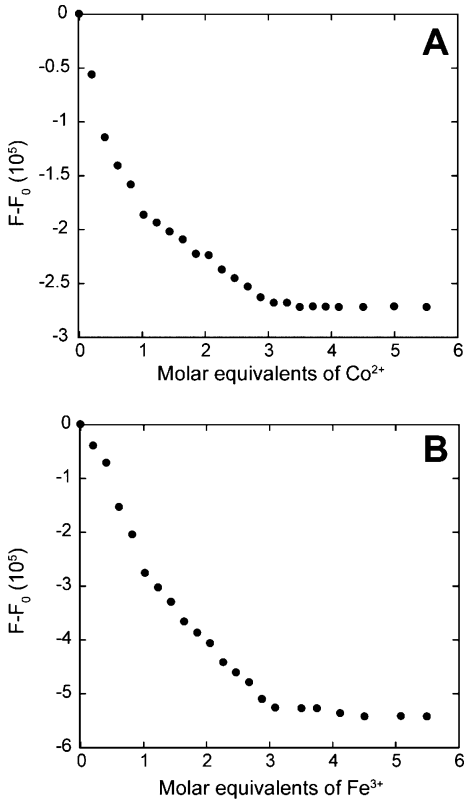

Figure 3. Fluorescence iron and cobalt titrations. Fluorescence emission spectra were recorded for metal titrations of 5 μM frataxin with an excitation at 295 nm. The corrected fluorescence intensity was plotted against the molar equivalents of Co^{2+} (A) and Fe^{3+} (B). In both cases, stoichiometric binding was observed with saturation at ~3 equiv of metal.

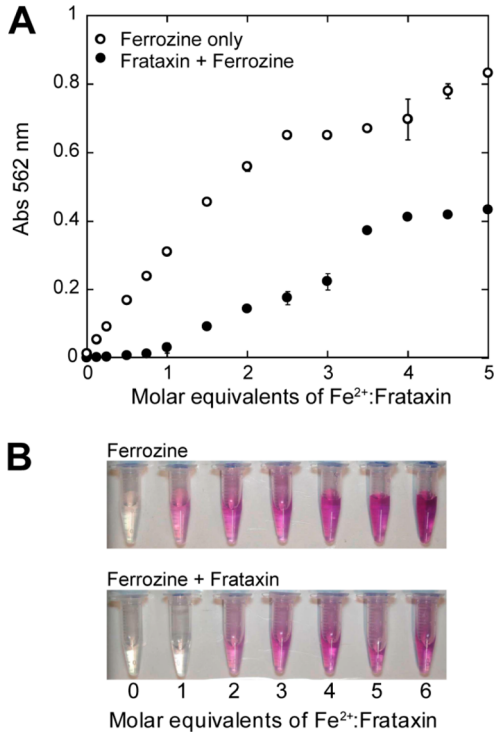

Figure 4. Ferrozine iron competition titration. (A) The binding isotherms at 562 nm for the ferrozine titrations without (○) and with 13 μM frataxin (●) are shown. (B) Shown are representative samples from a Fe^{2+} titration of 108 μM ferrozine (top) and 13 μM frataxin with 108 μM ferrozine (bottom). The ferrozine$_3$/Fe^{2+} complex is purple in color. Up to 1 mol equiv of Fe^{2+}, the metal preferentially binds to frataxin as shown by the lack of purple color and absorbance at 562 nm.

subsequent NMR titrations were preformed *without* Mg^{2+}. With increasing concentrations of Co^{2+} in the absence of Mg^{2+}, frataxin NMR resonances show significant line broadening. By ~3 equiv of Co^{2+}, resonances from the acidic α1 helix (D104, S105, E108, D112, L113, A114, D115) and others near it (Y118, V125, F127, V131) are no longer observable (Figure 5A). These residues are most likely within 8−15 Å of the bound Co^{2+} ions.[34] A plot of the change in normalized amide chemical shift (δ_{NH}) shows clustered shifting between residues 103−117 and 122−133, which are localized to α1−loop−β1. There are also smaller shifts for residues at the beginning of α1 (D91, A99).

We then compared the Co^{2+} HSQC spectra to those of Fe^{2+} collected anaerobically. High-spin Fe^{2+} broadens and shifts resonances within 5−7 Å of bound iron.[34] As shown in Figure 5B, the largest changes in normalized amide chemical shift after 2 equiv of Fe^{2+} localize to α1 (D104, S105, D112, L113, A114, D115) and into β1 (T119, D122, D124, V125). With 3 equiv of Fe^{2+}, D91, D104, and D122 undergo further chemical shifting. Many residues in α1 broaden but only D112, L113, and D115 broaden beyond detection at 3 mol equiv of Fe^{2+}. It is important to note that no significant changes in resonance intensities or chemical shift are observed beyond 3 equiv of Co^{2+} or Fe^{2+}.

HDX−MS. While NMR experiments have yielded valuable information about the localization of metal binding sites, it is still unclear whether frataxin undergoes changes in conformation or dynamics upon metal binding since there is no three-dimensional structure of any frataxin with metal bound. These changes could be important for interactions with potential protein partners such as ISCU and NFS1. We performed HDX−MS on apo−frataxin and frataxin with 1, 2, and 3 mol equiv of Co^{2+}, Fe^{2+}, or Fe^{3+}. HDX−MS monitors the rate of deuterium incorporation into amides within the protein backbone. The amount of deuterium exchanged into the backbone within the first 15 s of incubation mainly reports on accessibility of the amide hydrogen to D_2O and is a good indicator of secondary structure content (i.e., amide hydrogen bonding). Amides that exchange on a slower time scale are best attributed to dynamic motions and local unfolding/folding processes.[28] Deuterium incorporation as a function of time is detected through increased masses (m/z) of pepsin-digested peptides from exchange of ^1H with ^2H.

First, we investigated whether Co^{2+}, Fe^{2+} (~5% Fe^{3+}), and Fe^{3+} altered the solvent accessibility of amide hydrogens and whether the effects were metal specific. In general, decreased deuterium incorporation with 1 equiv of each metal was slight compared to that of apo-frataxin. The differences in HDX become more pronounced with the second and third equivalents of metal, which indicates distribution between all three binding sites. No additional changes in HDX are observed beyond 3 equiv of metal. The percent change in amide deuteration with 2 and 3 equiv of metal are shown in Figure 6. Peptides from the N-terminus (residues 81−91), in β1 (residues 122−127), and within the β4−β5 strands (residues 156−172) showed reduced deuterium incorporation for all metal ions. Fe^{3+} also displayed a change within residues 128−

dx.doi.org/10.1021/bi400443n | *Biochemistry* 2013, 52, 6085−6096

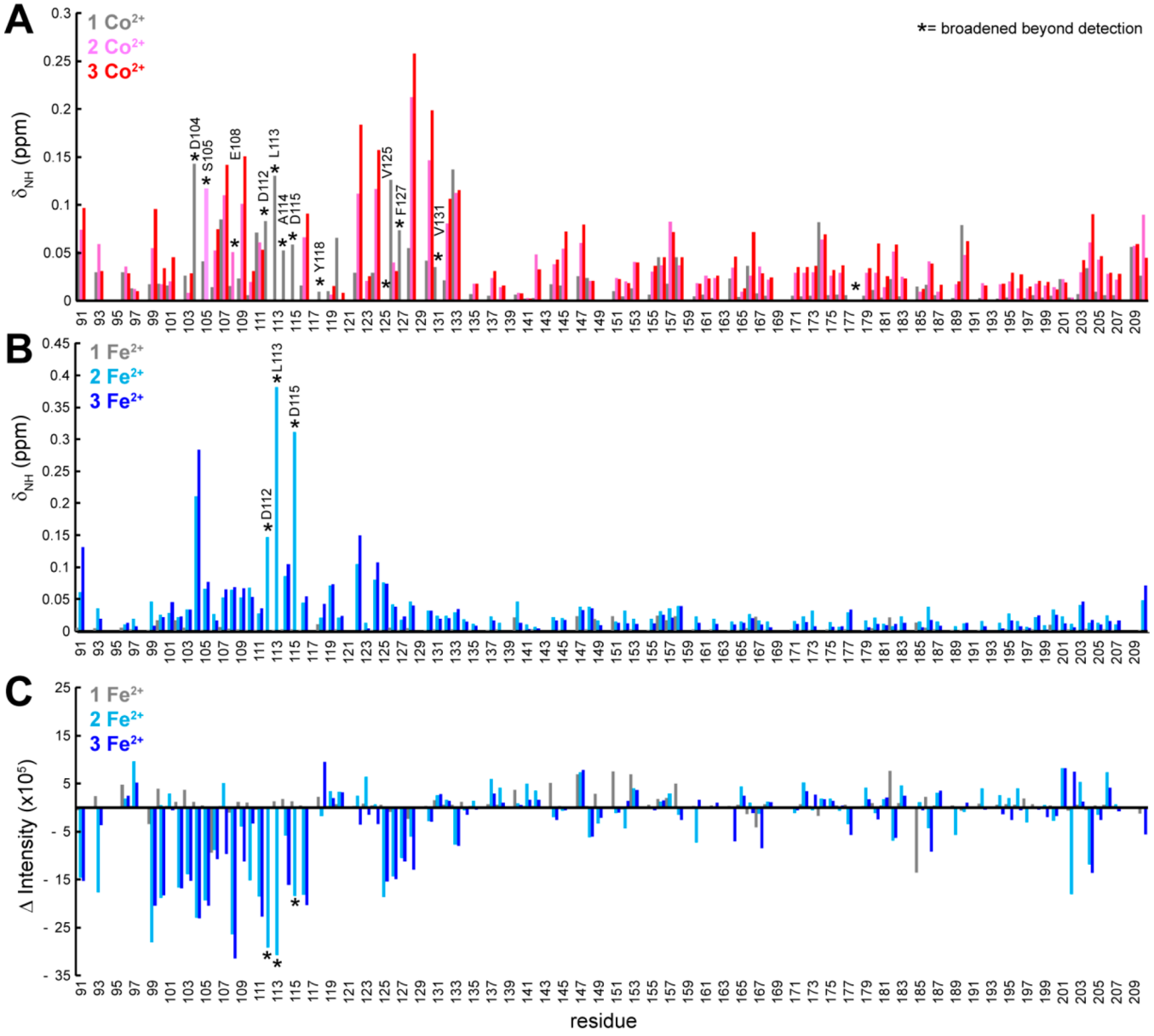

Figure 5. NMR titrations of frataxin with cobalt and iron. (A) The changes in normalized amide chemical shift (δ_{NH}) of 560 μM ^{15}N-frataxin with 1, 2, and 3 mol equiv of Co^{2+} are in gray, pink, and red, respectively. (B) The change in normalized amide chemical shift (δ_{NH}) of 560 μM ^{15}N-frataxin with 1, 2, and 3 mol equiv of Fe^{2+} are in gray, cyan, and dark blue, respectively. Samples were made anaerobically. (C) The changes in intensity of ^{1}H−^{15}N-frataxin resonances upon addition of 1, 2, and 3 mol equiv of Fe^{2+} are in gray, cyan, and dark blue, respectively. Asterisks denote the positions of the amino acids whose resonances broadened beyond detection during the titrations.

132 that was not observed with Fe^{2+} or Co^{2+}. The third equivalent of metal further protected amides within α1 and β1 (81−91, 91−98, 110−121 and 122−127). These peptides are mapped on the frataxin structure with the exception of residues 81−90, which were not observed in the NMR structure (Figure 6B−G).[12] It is also interesting to note that metal binding alters deuterium exchange in the β4−β5 strands, which are thought to interact with the Fe−S cluster machinery.[12] This indicates that metal coordination affects frataxin conformation beyond the immediate binding vicinity.

In addition to changes in amide D_2O accessibility, HDX rates can be correlated to altered local dynamics or structure upon metal binding that could be functionally relevant. We compared the HDX progress curves for only Co^{2+} and Fe^{3+}-frataxin samples. The signal-to-noise of the mass spectra for Fe^{2+}-frataxin decreased as a function of time presumably from iron oxidation and was not pursued further. HDX deuterium incorporation rate profiles for all pepsin generated peptides with both Co^{2+} and Fe^{3+} were comparable (Figure S3 in Supporting Information), but only Fe^{3+} progress curves are shown (Figure 7). Addition of 2 and 3 mol equiv of Fe^{3+} to frataxin leads to a conformational change in the β4-β5 sheets (peptide 156−172) that affects protein dynamics and solvent accessibility. Other notable decreases in rate were observed for the N-terminus (peptide 81−91) and α1-β1 (peptides 91−98, 99−103, 110−123). Given that the N-terminus is disordered, we sought to better understand why residues 81−91 displayed such a large change in solvent accessibility and conformational dynamics upon metal binding. It is possible that residues in the

dx.doi.org/10.1021/bi400443n | Biochemistry 2013, 52, 6085−6096

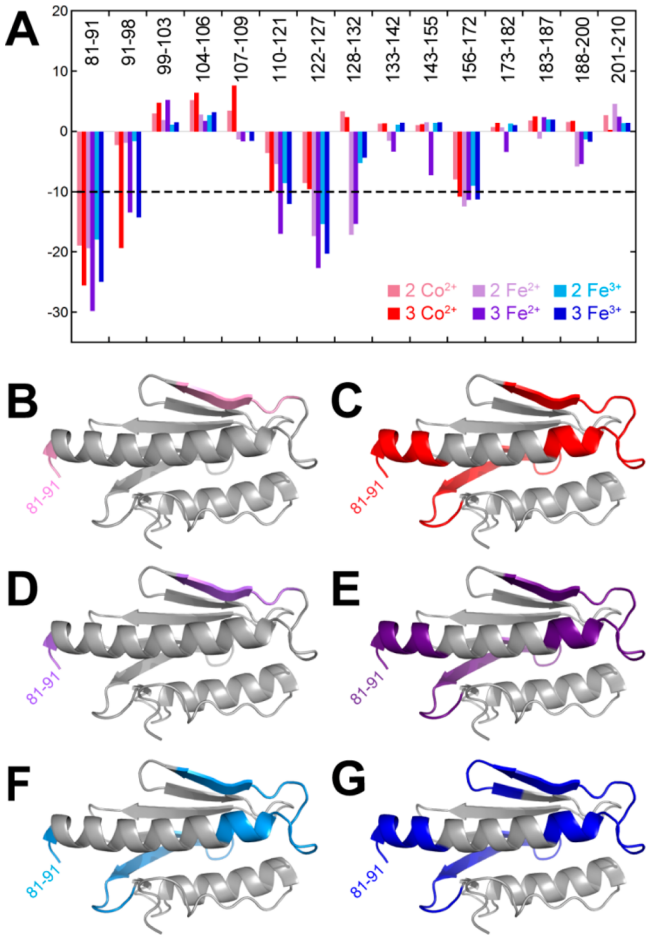

Figure 6. (A) HDX–MS titrations with cobalt and iron. The D_2O accessibility of backbone amides was determined by the percentage of amides exchanging with rates greater than 4 min^{-1} for each pepsin-generated peptide. The percentage exchanged for apo-frataxin was subtracted from the percentage obtain with 2 and 3 equiv of metal: $2Co^{2+}$ (pink); $3Co^{2+}$ (red); $2Fe^{2+}$ (light purple); $3Fe^{2+}$ (purple); $2Fe^{3+}$ (cyan); $3Fe^{3+}$ (blue). (B–G) Peptides that have HDX changes greater than 10% at 3 equiv of metal are mapped to the structure of 91–210 frataxin (PDB: 1EKG)[42] using the color scheme in panel A. Note the HDX data includes peptide 81–91, which is not observed in the structure.

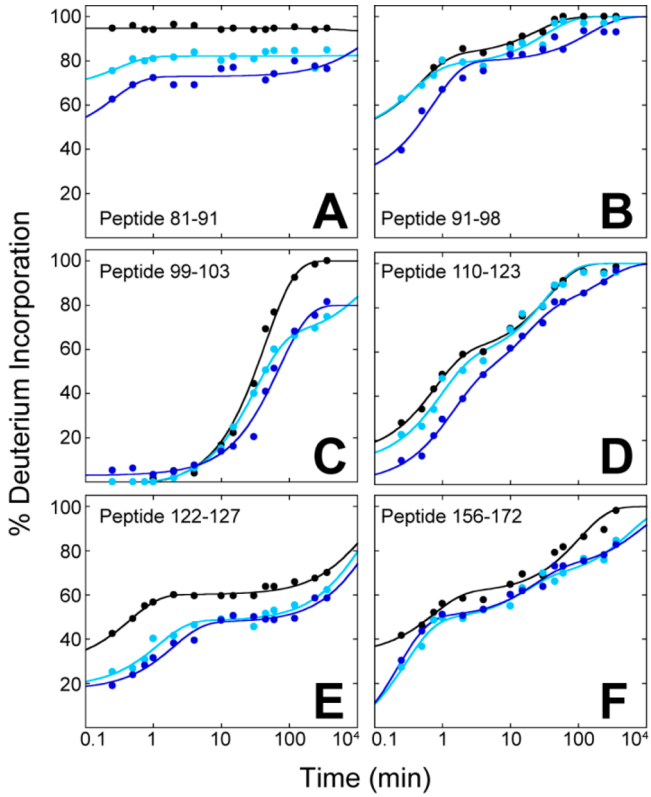

Figure 7. HDX–MS rate profiles for selected frataxin peptides. Shown are the kinetic traces for the % deuterium incorporated into peptides derived from apo- (black), $2Fe^{3+}$- (cyan), and $3Fe^{3+}$-(blue) frataxin as a function of incubation time in D_2O. (A) Peptide 81–91. (B) Peptide 91–98. (C) Peptide 99–103. (D) Peptide 110–123. (E) Peptide 122–127. (F) Peptide 156–172. The data were averaged from three experiments and were fit to single or double exponential equations to obtain the rate constants for exchange (k_n) and the corresponding percentage of deuterons in each phase ($\%D_n$). The fitted parameters are given in Table 1. The corresponding HDX–MS plots for $2Co^{2+}$- and $3Co^{2+}$-frataxin samples are in Supporting Information.

N-terminus could be involved in metal-promoted aggregation, as observed in Yfh1 studies,[35] or direct metal coordination.

Mutagenesis of His86 in the N-Terminal Region. Analytical size exclusion chromatography with frataxin preincubated with up to 10 mol equiv of Co^{2+} or Fe^{3+} does not indicate stabile oligomerization (Figure S4, Supporting Information), consistent with other studies.[36] To test for direct metal coordination, site-directed mutagenesis of potential metal binding ligands was pursued. Within residues 81–91, His86 is the only residue to commonly coordinate metals, so His86 was mutated to alanine and characterized. Co^{2+} absorption spectroscopy is sensitive enough to detect changes in coordination environment.[32] The d–d transitions for H86A frataxin with Co^{2+} shift to higher energies and with decreased molar absorptivity, compared to wild-type frataxin (Figure 8A). Analysis of the Co^{2+} binding isotherm for H86A frataxin reveals saturation after ~2 equiv (Figure 8B); therefore, substitution of His86 leads to loss of one metal binding site. H86A frataxin was also titrated with Fe^{2+} in the presence of ferrozine chelator (Figure 8C,D). In contrast to wild-type, ferrozine out-competes H86A frataxin for Fe^{2+}. This demonstrates that His86 is a ligand in the higher affinity Fe^{2+} site observed for the wild-type protein.

Fe–S Cluster Assembly. Although mutagenesis of His86 resulted in a loss of a single metal binding site, it was not clear whether this had functional relevance. ISCU is a Fe–S scaffold protein that assembles [2Fe-2S] clusters on its surface using free Fe^{2+} and sulfide. The presence of iron-bound frataxin enhances the rate of cluster assembly *in vitro*.[7] This assay was used to determine if mutation of His86 affected the rate of Fe–S cluster synthesis (Figure 9). In the presence of free Fe^{2+}, ISCU assembled a cluster with a basal initial rate of 0.018 s^{-1}; however, the rate was ~4-fold greater in the presence of wild-type frataxin preincubated with 2 equiv of Fe^{2+} (0.074 s^{-1}). When H86A frataxin with 2 equiv of Fe^{2+} was used, the rate of Fe–S formation is similar to the basal level (0.018 s^{-1}). Incubation of H86A frataxin with >2 equiv of Fe^{2+} did not increase the rate of Fe–S synthesis (data not shown). These data suggest that the H86A mutation negates the stimulatory effect by frataxin on Fe–S cluster biogenesis. To elucidate if the loss of Fe–S rate enhancement from the H86A mutation could be from decreased affinity for ISCU, intrinsic tryptophan fluorescence quenching titrations of ISCU into frataxin were

dx.doi.org/10.1021/bi400443n | *Biochemistry* 2013, 52, 6085–6096

Table 1. HDX−MS Rate Constants and Amplitudes for Peptides from Figure 7[a]

peptide	$\%D_{Pre\text{-}Ex}$[b]	$\%D_1$	k_1 (min^{-1}) "fast"	$\%D_2$	k_2 (min^{-1}) "intermediate"	$\%D_3$	k_3 (min^{-1}) "slow"
81−91							
apo	~100						
2 Fe^{3+}	~81					17.8 (±1.0)	$\leq 1 \times 10^{-4}$
3 Fe^{3+}	~73					27.0 (±1.4)	$\leq 1 \times 10^{-4}$
91−98							
apo	~47	35.7 (±4.5)	2.2 (±0.4)	17.5 (±1.3)	0.040 (±0.007)		
2 Fe^{3+}	~47	31.5 (±11.2)	2.7 (±1.2)	21.9 (±2.2)	0.031 (±0.007)		
3 Fe^{3+}	~26	53.3 (±8.8)	1.4 (±0.4)	20.3 (±2.4)	0.007 (±0.002)		
99−103							
apo	0			100 (±1.2)	0.022 (±0.001)		
2 Fe^{3+}	0			67.1 (±2.6)	0.032 (±0.002)	~33	$\leq 1 \times 10^{-4}$
3 Fe^{3+}	0			76.9 (±1.5)	0.014 (±0.001)	~23	$\leq 1 \times 10^{-4}$
110−123							
apo	~23	36.8 (±5.0)	1.1 (±0.3)	40.1 (±2.3)	0.018 (±0.002)		
2 Fe^{3+}	~12	34.3 (±5.0)	1.4 (±0.4)	38.1 (±3.6)	0.06 (±0.01)	15.6 (±3.3)	0.002 (±0.001)
3 Fe^{3+}	~2	28.7(±7.5)	2.0 (±1.0)	32.5 (±3.9)	0.10 (±0.02)	37.4 (±2.4)	0.0030 (±0.0005)
122−127							
apo	~29	31 (±4)	2.2 (±0.4)			40 (±0.5)	$\leq 1 \times 10^{-4}$
2 Fe^{3+}	~18	30 (±4)	0.9 (±0.2)			52 (±1)	$\leq 1 \times 10^{-4}$
3 Fe^{3+}	~18	30 (±3)	0.5 (±0.1)			52 (±1)	$\leq 1 \times 10^{-4}$
156−172							
apo	~33	28 (±7)	1.4 (±0.6)	39 (±2)	0.010 (±0.002)		
2 Fe^{3+}	~25	24 (±9)	2.1 (±0.5)	19 (±4)	0.06 (±0.04)	32 (±4)	0.0017 (±0.0005)
3 Fe^{3+}	~29	21 (±2)	2.3 (±0.5)	22 (±3)	0.05 (±0.01)	28 (±3)	0.0012 (±0.0005)

[a]Parameters obtained from fitting the H/D-exchange kinetics of frataxin peptides with and without metal (Figure 7A−F) according to a single, double or triple exponential equations. The rates have been loosely grouped in to fast, intermediate and slow exchange. [b]The amount of exchange before the first time point is estimated from the fit parameters and is assigned a rate of exchange >4 min^{-1}.[28]

performed with and without Fe^{3+}, as described.[37] The fluorescence of wild type and H86A frataxin was quenched by ISCU only in the presence of Fe^{3+} (Figure S5, Supporting Information). H86A only had a 2-fold lower K_D for ISCU than for wild type frataxin. Together, these studies show that His86 is important for iron binding and in the formation of Fe−S clusters by ISCU *in vitro* but does not seem to play a direct role in ISCU binding.

DISCUSSION

Human frataxin is a unique Fe^{2+}-binding protein in that the mature form does not contain cysteine residues, which are preferred ligands based on hard−soft acid base theory.[38] Instead, a cluster of aspartate and glutamate residues along one face of α1 helix creates multiple binding sites for Fe^{2+} (Figure 1).[11] This region has hampered direct determination of frataxin metal stoichiometry from a variety of approaches since its interactions with metals could also be nonspecific. For a better understanding of frataxin molecular interactions, metal coordination as related to structure and function was investigated. From this study, we propose that His86 is a previously unidentified iron ligand and that it plays a functional role in Fe−S synthesis with the scaffold protein ISCU.

Localization of Metal Binding Sites in Frataxin Using Paramagnetic NMR and HDX-MS. Our studies cumulatively suggest that mature frataxin can bind up to three metal ions. One Fe^{2+} binding site has higher affinity than the other two sites based on chelator competition assays. In these studies, a significant population of "free" metal exists so differences in affinity can be discerned. In other experiments, the frataxin concentration is high enough that stoichiometric binding was observed. It also led to metal distribution among all three sites. At this time, it is not possible to determine if the two weaker metal binding sites observed in this study are nonspecific because actual equilibrium binding constants have not been determined. Further functional roles for these residues must be ascertained. The HSQC NMR metal titrations in the presence of Mg^{2+} attempted to control nonspecific metal coordination, but Mg^{2+} competed with Co^{2+} for binding at or near acidic residues within α1−loop−β1 (Figure S1, Supporting Information). This suggests that electrostatic interactions with the acidic α1 helix are possible.[18] Some of these acidic residues are important for interaction with ISCU and other components of the Fe−S machinery and not for iron binding.[9]

When the Co^{2+} and Fe^{2+} NMR results with 81−210 frataxin are compared with those for truncated human frataxin (residues 91−210), *S. cerevisiae* Yfh1, and *E. coli* CyaY, similarities are observed that allow for the assignment of several potential ligands (Figure 10). D112 and D115 from the α1 helix are likely metal coordinating residues since their NMR resonances were broadened beyond detection with Co^{2+} and Fe^{2+} in our experiments and in other homologues (Figure 10).[13,14,18] Acidic residues at positions 112 and 115 are conserved in most eukaryotic frataxins.[11] HDX−MS studies showed that the peptide containing D112 and D115 (110−123) incorporated less deuterium into the backbone in the presence of metal (Figure 7D). In combination with NMR results, this is consistent with reduced solvent accessibility and dynamics from metal coordination.[39]

HDX−MS also revealed that amides within residues 122−127 in β1 were protected from D_2O in the presence of metal without a measurable change in the rate of uptake (Figure 7E). In other words, metal binding does not significantly perturb structure in β1. Several residues in this region had altered NMR

dx.doi.org/10.1021/bi400443n | *Biochemistry* 2013, 52, 6085−6096

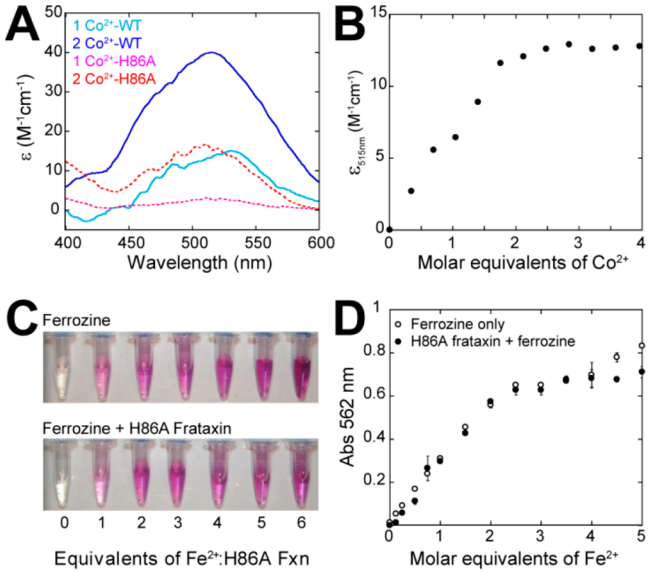

Figure 8. Cobalt and iron binding to H86A frataxin. (A) Shown are representative spectra plotted in molar absorptivity (ε) of wild-type and H86A frataxin with Co^{2+} bound. Wild-type frataxin (solid lines) with 1 and 2 equiv of Co^{2+} are in cyan and blue, respectively. H86A frataxin (dashed lines) with 1 and 2 equiv of Co^{2+} are in pink and red, respectively. Both a loss of molar absorptivity and a shift in the λ_{max} is observed with H86A frataxin. (B) After correcting the data for nonspecific binding, the isotherm indicates H86A frataxin coordinates ~2 equiv of Co^{2+} per protein. (C) Shown are representative samples from a Fe^{2+} titration of 108 μM ferrozine (top panel) and 13 μM H86A frataxin with 108 μM ferrozine (bottom panel). The ferrozine$_3$/Fe^{2+} complex is purple in color. (D) The binding isotherms at 562 nm for the ferrozine titrations without (○) and with H86A frataxin (●) described in (C) are shown. Fe^{2+} preferentially binds to ferrozine even in the presence of H86A frataxin.

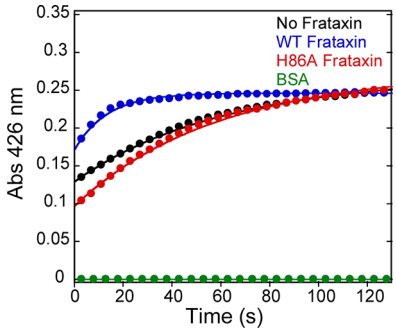

Figure 9. Functional interaction between frataxin and ISCU. (A) Shown are averaged progress curves for the assembly of [2Fe–2S] clusters by D37A ISCU (100 μM) using various Fe^{2+} donors in excess sodium sulfide. The anaerobic reaction progress curves were followed at 426 nm and were initiated by 200 μM Fe^{2+} as "free" metal in the absence of protein (black), $2Fe^{2+}$–frataxin (blue), $2Fe^{2+}$–H86A frataxin (red), or $2Fe^{2+}$–BSA (green). The curves were fit to first-order rate equations to obtain the initial rate of Fe–S cluster assembly.

chemical shifts and broadening in the presence of Co^{2+} and Fe^{2+}, including D122 and D124, but the magnitude was smaller than D112 and D115. D122 and D124 are highly conserved and appear to coordinate Co^{2+} and Fe^{2+} in human, *S. cerevisiae*, and *E. coli* frataxins (Figure 10).[11,13,14] Interaction studies of mutant frataxin proteins with the ISCU/NFS1/ISD11 ternary complex showed that D124 of frataxin was essential for interaction.[9] It is not apparent if iron coordination to D124 mediates the interaction or if the residue is available to coordinate iron when frataxin is bound to the Fe–S machinery. It has been noted that "free" frataxin binds less iron than and frataxin in complex with ISCU/NFS1/ISD11, supporting the latter prediction, but more specific binding studies are required.[10]

Large decreases in solvent accessibility and slower rates of deuterium incorporation were also observed for peptides 81–91 (N-terminus) and 91–98 (beginning of α1). In fact, 81–91 had the largest overall decrease in D_2O accessibility of any peptide, especially at 2 equiv of metal (Figure 6A). Resonances of residues 81–90 from the disordered N-terminus were not observed in NMR structures of human frataxin, so metal coordination to residues within 81–90 could not be obtained.[12] Thus, further studies were required to ascertain if residue(s) in the N-terminal region can coordinate metals.

His86 Is a Potential Metal Ligand and Is Required for Fe–S Synthesis by ISCU. Investigation into why the N-terminus showed a conformational response with metal suggested that it was from direct metal coordination. Specifically, mutation of His86 to alanine led to loss of one of the three identified metal binding sites and a shift in the Co^{2+} *d-d* transitions, suggesting a change in coordination environment such as loss of a nitrogen-containing ligand.[32,33] Ferrozine competition assays suggested that the higher affinity Fe^{2+} binding site was lost in the H86A mutant. It has been assumed that because the N-terminal "extension" before α1 is not found in bacteria and has weak conservation in eukaryotes, that residues within it are not functionally relevant.[11] Our studies revealed a functional role for His86 in Fe–S synthesis *in vitro* since H86A frataxin did not stimulate Fe–S cluster biogenesis by ISCU. Sequence alignments reveal a lack of conservation of His86 across all frataxin homologues. Some higher eukaryotes and yeast have a metal coordinating residue such as histidine, glutamate, or aspartate aligned with human frataxin residue His86 (Supporting Information, Figure S6A), which is intriguing, but unclear if it is related to intracellular function at this time.[11] Clearly, research into the *in vivo* relevance of His86 is required.

It is well established that the N-terminus of eukaryotic frataxins is processed for mitochondrial localization, leaving the N-terminal extension before α1.[40] The intermediate processed form of frataxin (residues 46–210) undergoes iron-mediated self-cleavage to produce mature frataxin. It is intriguing that the intermediate form had one high affinity Fe^{2+} binding site ($K_d \leq$ 300 nM).[41] Iron-dependent cleavage of the N-terminal domain to form 78–210 frataxin led to additional, lower affinity iron binding sites. Yoon et al. proposed that the unprocessed N-terminus in 46–210 frataxin could interact with the α1 carboxylate residues to block iron binding along the acidic ridge.[41] This observation is somewhat consistent with our results showing ~3 Fe^{2+} binding sites in 81–210 frataxin, one with higher affinity. There is no structure of the human intermediate with the extended N-terminus; however, a structure of the intermediate form of yeast frataxin, Yfh1 (residues 53–174, yeast numbering), revealed that the disordered N-terminus (residues 53–69, yeast numbering) extended over α1 (Supporting Information, Figure S6B).[14] On the basis of this structure and a protein alignment (Supporting Information, Figure 6A), His86 in human 81–210 frataxin would be too far away from residues D112, D115, D122, and D124 to form a binding site, but it is within interaction distance to residues at the beginning of α1 such as D91. Our Co^{2+} and

dx.doi.org/10.1021/bi400443n | *Biochemistry* 2013, 52, 6085–6096

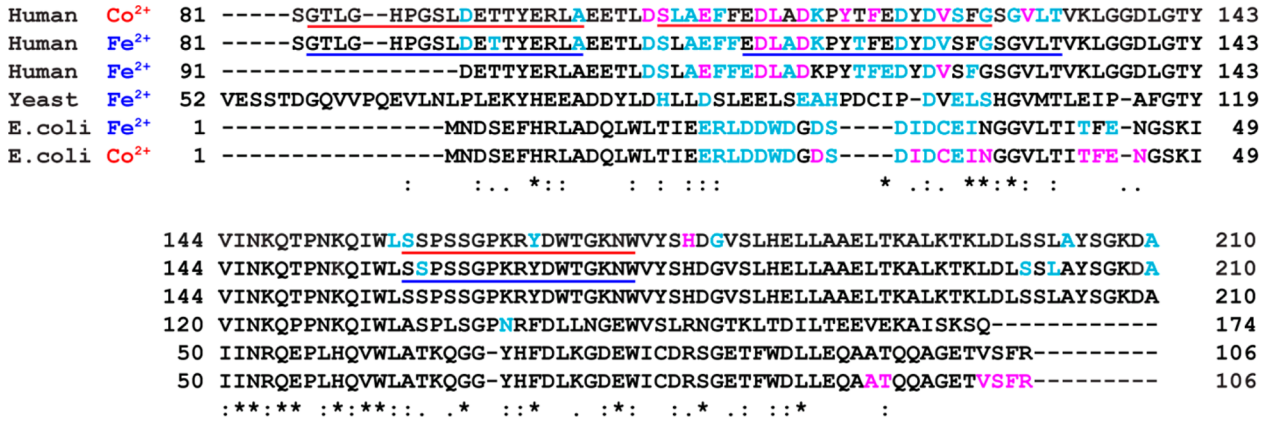

Figure 10. Summary of NMR titrations of frataxin homologues. An alignment of mature *H. sapiens* frataxin, *S. cerevisiae* Yfh1, and *E. coli* CyaY proteins was created with ClustalW,[43] and the residues shown to broaden beyond detection (magenta) or have large chemical shifts (cyan) in Fe^{2+} or Co^{2+} NMR titrations are indicated. The first and second entries (81−210 human frataxin) are from this study, the third entry (91−210 human frataxin) is from Nair et al.,[13] the fourth entry (52−174 yeast Yfh1) is from He et al.,[14] and the fifth and sixth entries (1−106 *E. coli* CyaY) are from Pastore et al.[18] The lines under the amino acid sequence indicate peptides that had decreased deuterium incorporation in HDX−MS experiments with Fe^{3+} (blue) and Co^{2+} (red).

Fe^{2+} NMR titrations indicated broadening and shifting of resonances at the beginning of α1 (D91, T93) of about the same magnitude as those for D122 and D124. Our results warrant further study into the role of His86 and potentially other residues near the N-terminus that could form an iron binding site.

CONCLUSIONS

Using a variety of spectroscopic and structural approaches, we describe the identification of His86 as a new iron coordinating residue in the unstructured N-terminus of human frataxin. Further studies revealed that His86 is required for efficient Fe−S cluster synthesis with ISCU; however, additional mutagenesis and *in vivo* characterization is required to further clarify the biological role of this residue in the synthesis of Fe−S clusters. Our results question the functional relevance of iron binding at residues within the acidic α1 helix and support the possibility that residues in the N-terminus could be relevant to Fe−S cluster synthesis as part of the quaternary complex with ISCU/NSF1/ISD11.

ASSOCIATED CONTENT

Supporting Information

Figure S1 (NMR chemical shift and intensity Co^{2+} binding isotherms with and without Mg^{2+}); Figure S2 (changes in intensity and chemical shift upon addition of Mg^{2+}); Figure S3 (HDX−MS rate profiles for all frataxin peptides); Figure S4 (analytical size exclusion chromatography of frataxin with Co^{2+} and Fe^{3+}); Figure S5 (fluorescence titrations of wild type and H86A frataxin with ISCU); Figure S6 (frataxin sequence alignment and overlaid human and yeast frataxin structures); Table S1 (HDX−MS rate constants and amplitudes for peptides from Figure S3); Table S2 (analytical size exclusion calculated molecular weights from Figure S4). This material is available free of charge via the Internet at http://pubs.acs.org.

AUTHOR INFORMATION

Corresponding Author

*E-mail: LSBusenlehner@bama.ua.edu. Phone: (205) 348-0269. Fax: (205) 348-9104.

Present Address

‡Resident Physician in Internal Medicine, David Geffen School of Medicine, University of California at Los Angeles, Los Angeles, CA 90095.

Funding

This work was supported by National Science Foundation Grant MCB 0845273 (L.S.B), National Science Foundation CRIF Grant CHE 0639003, and National Institutes of Health Grant R01 GM030910 (R.N.A.).

Notes

The authors declare no competing financial interest.

ACKNOWLEDGMENTS

The authors would like to thank the Department of Chemistry Mass Spectrometry Resource Facility manager, Dr. Qiaoli Liang, and NMR Facility manager, Dr. Ken Belmore, for assistance with instrumentation. We also thank Prof. Richard Armstrong for allowing initial HDX−MS studies with frataxin to be conducted at Vanderbilt University.

ABBREVIATIONS

$\varepsilon_{280\ nm}$, molar extinction coefficient at 280 nm; Bis-Tris, 2,2-bis(hydroxymethyl)-2,2′,2″-nitrilotriethanol; CyaY, bacterial frataxin homologue; d_{18}-HEPES, deuterated 4-(2-hydroxyethyl)piperazine-1-ethanesulfonic acid; EDTA, ethylenediaminetetraacetic acid; FA, Friedreich's Ataxia; Fe−S cluster, iron−sulfur cluster; HDX−MS, hydrogen/deuterium exchange mass spectrometry; HEPES, 4-(2-hydroxyethyl)-piperazine-1-ethanesulfonic acid; HPLC, high performance liquid chromatography; HSQC, heteronuclear single-quantum coherence; IPTG, isopropyl β-D-1-thiogalactopyranoside; ISCU, human iron−sulfur cluster scaffold protein; ISD11, human iron−sulfur cluster accessory protein; K_D, equilibrium dissociation constant; K_f, formation constant; MALDI−TOF, matrix assisted laser desorption/ionization−time-of-flight; MS, mass spectrometry; MS/MS, tandem mass spectrometry; NFS1, human cysteine desulfurase; NMR, nuclear magnetic resonance; $OD_{600\ nm}$, optical density at 600 nm; Yfh1, yeast frataxin homologue

REFERENCES

(1) Campuzano, V., Montermini, L., Molto, M. D., Pianese, L., Cossee, M., Cavalcanti, F., Monros, E., Rodius, F., Duclos, F., Monticelli, A., Zara, F., Canizares, J., Koutnikova, H., Bidichandani, S. I., Gellera, C., Brice, A., Trouillas, P., De Michele, G., Filla, A., De Frutos, R., Palau, F., Patel, P. I., Di Donato, S., Mandel, J. L., Cocozza, S., Koenig, M., and Pandolfo, M. (1996) Friedreich's ataxia: autosomal recessive disease caused by an intronic GAA triplet repeat expansion. *Science 271*, 1423−1427.

(2) Schmucker, S., and Puccio, H. (2010) Understanding the molecular mechanisms of Friedreich's ataxia to develop therapeutic approaches. *Hum. Mol. Genet. 19*, R103−110.

(3) Gonzalez-Cabo, P., Llorens, J. V., Palau, F., and Molto, M. D. (2009) Friedreich ataxia: an update on animal models, frataxin function and therapies. *Adv. Exp. Med. Biol. 652*, 247−261.

(4) Rouault, T. A., and Tong, W. H. (2008) Iron-sulfur cluster biogenesis and human disease. *Trends Genet. 24*, 398−407.

(5) Ye, H., and Rouault, T. A. (2010) Human iron-sulfur cluster assembly, cellular iron homeostasis, and disease. *Biochemistry 49*, 4945−4956.

(6) Muhlenhoff, U., Richhardt, N., Ristow, M., Kispal, G., and Lill, R. (2002) The yeast frataxin homolog Yfh1p plays a specific role in the maturation of cellular Fe/S proteins. *Hum. Mol. Genet. 11*, 2025−2036.

(7) Kondapalli, K. C., Kok, N. M., Dancis, A., and Stemmler, T. L. (2008) Drosophila frataxin: an iron chaperone during cellular Fe-S cluster bioassembly. *Biochemistry 47*, 6917−6927.

(8) Watson, H. M., Gentry, L. E., Asuru, A. P., Wang, Y., Marcus, S., and Busenlehner, L. S. (2012) Heterotrifunctional chemical cross-linking mass spectrometry confirms physical interaction between human frataxin and ISU. *Biochemistry 51*, 6889−6891.

(9) Schmucker, S., Martelli, A., Colin, F., Page, A., Wattenhofer-Donze, M., Reutenauer, L., and Puccio, H. (2011) Mammalian frataxin: an essential function for cellular viability through an interaction with a preformed ISCU/NFS1/ISD11 iron-sulfur assembly complex. *PLoS One 6*, e16199.

(10) Colin, F., Martelli, A., Clemancey, M., Latour, J. M., Gambarelli, S., Zeppieri, L., Birck, C., Page, A., Puccio, H., and Ollagnier de Choudens, S. (2013) Mammalian Frataxin Controls Sulfur Production and Iron Entry during de Novo Fe(4)S(4) Cluster Assembly. *J. Am. Chem. Soc. 135*, 733−740.

(11) Pandolfo, M., and Pastore, A. (2009) The pathogenesis of Friedreich ataxia and the structure and function of frataxin. *J. Neurol. 256* (Suppl 1), 9−17.

(12) Musco, G., Stier, G., Kolmerer, B., Adinolfi, S., Martin, S., Frenkiel, T., Gibson, T., and Pastore, A. (2000) Towards a structural understanding of Friedreich's ataxia: the solution structure of frataxin. *Structure 8*, 695−707.

(13) Nair, M., Adinolfi, S., Pastore, C., Kelly, G., Temussi, P., and Pastore, A. (2004) Solution structure of the bacterial frataxin ortholog, CyaY: mapping the iron binding sites. *Structure 12*, 2037−2048.

(14) He, Y., Alam, S. L., Proteasa, S. V., Zhang, Y., Lesuisse, E., Dancis, A., and Stemmler, T. L. (2004) Yeast frataxin solution structure, iron binding, and ferrochelatase interaction. *Biochemistry 43*, 16254−16262.

(15) Cook, J. D., Bencze, K. Z., Jankovic, A. D., Crater, A. K., Busch, C. N., Bradley, P. B., Stemmler, A. J., Spaller, M. R., and Stemmler, T. L. (2006) Monomeric yeast frataxin is an iron-binding protein. *Biochemistry 45*, 7767−7777.

(16) Lane, D. J., and Richardson, D. R. (2010) Frataxin, a molecule of mystery: trading stability for function in its iron-binding site. *Biochem. J. 426*, e1−3.

(17) Huang, J., Dizin, E., and Cowan, J. (2008) Mapping iron binding sites on human frataxin: implications for cluster assembly on the ISU Fe−S cluster scaffold protein. *J. Biol. Inorg. Chem 13*, 825−836.

(18) Pastore, C., Franzese, M., Sica, F., Temussi, P., and Pastore, A. (2007) Understanding the binding properties of an unusual metal-binding protein–a study of bacterial frataxin. *FEBS. J. 274*, 4199−4210.

(19) Maret, W., and Vallee, B. L. (1993) Cobalt as probe and label of proteins. *Methods Enzymol. 226*, 52−71.

(20) Thompsen, J. C., and Mottola, H. A. (1984) Kinetics of the Complexation of Iron(II) with Ferrozine. *Anal. Chem. 56*, 755−757.

(21) van de Weert, M. (2010) Fluorescence quenching to study protein-ligand binding: common errors. *J. Fluoresc. 20*, 625−629.

(22) Musco, G., de Tommasi, T., Stier, G., Kolmerer, B., Bottomley, M., Adinolfi, S., Muskett, F. W., Gibson, T. J., Frenkiel, T. A., and Pastore, A. (1999) Assignment of the 1H, 15N, and 13C resonances of the C-terminal domain of frataxin, the protein responsible for Friedreich ataxia. *J. Biomol. NMR 15*, 87−88.

(23) Kay, L., Keifer, P., and Saarinen, T. (1992) Pure absorption gradient enhanced heteronuclear single quantum correlation spectroscopy with improved sensitivity. *J. Am. Chem. Soc. 114*, 10663−10665.

(24) Delaglio, F., Grzesiek, S., Vuister, G. W., Zhu, G., Pfeifer, J., and Bax, A. (1995) NMRpipe: A multidimensional spectral processing system based on Unix pipes. *J. Biomol. NMR 6*, 227−293.

(25) Grzesiek, S., Stahl, S. J., Wingfield, P. T., and Bax, A. (1996) The CD4 determinant for downregulation by HIV-1 Nef directly binds to Nef. Mapping of the Nef binding surface by NMR. *Biochemistry 35*, 10256−10261.

(26) Ma, B., Zhang, K., Hendrie, C., Liang, C., Li, M., Doherty-Kirby, A., and Lajoie, G. (2003) PEAKS: powerful software for peptide de novo sequencing by tandem mass spectrometry. *Rapid Commun. Mass Spectrom. 17*, 2337−2342.

(27) Engen, J. R., and Smith, D. L. (2001) Investigating protein structure and dynamics by hydrogen exchange MS. *Anal. Chem. 73*, 256A−265A.

(28) Busenlehner, L. S., and Armstrong, R. N. (2005) Insights into enzyme structure and dynamics elucidated by amide H/D exchange mass spectrometry. *Arch. Biochem. Biophys. 433*, 34−46.

(29) Tong, W. H., and Rouault, T. A. (2006) Functions of mitochondrial ISCU and cytosolic ISCU in mammalian iron-sulfur cluster biogenesis and iron homeostasis. *Cell Metab. 3*, 199−210.

(30) Solomon, E. I., Brunold, T. C., Davis, M. I., Kemsley, J. N., Lee, S. K., Lehnert, N., Neese, F., Skulan, A. J., Yang, Y. S., and Zhou, J. (2000) Geometric and electronic structure/function correlations in non-heme iron enzymes. *Chem. Rev. 100*, 235−350.

(31) Krezel, A., Lesniak, W., Jezowska-Bojczuk, M., Mlynarz, P., Brasuñ, J., Kozlowski, H., and Bal, W. (2001) Coordination of heavy metals by dithiothreitol, a commonly used thiol group protectant. *J. Inorg. Biochem. 84*, 77−88.

(32) Bertini, I., and Luchinat, C. (1984) High spin cobalt(II) as a probe for the investigation of metalloproteins. *Adv. Inorg. Biochem. 6*, 71−111.

(33) Dian, C., Vitale, S., Leonard, G. A., Bahlawane, C., Fauquant, C., Leduc, D., Muller, C., de Reuse, H., Michaud-Soret, I., and Terradot, L. (2011) The structure of the Helicobacter pylori ferric uptake regulator Fur reveals three functional metal binding sites. *Mol. Microbiol. 79*, 1260−1275.

(34) Otting, G. (2010) Protein NMR using paramagnetic ions. *Annu. Rev. Biophys. 39*, 387−405.

(35) Li, H., Gakh, O., Smith, D. Y. t., and Isaya, G. (2009) Oligomeric yeast frataxin drives assembly of core machinery for mitochondrial iron-sulfur cluster synthesis. *J. Biol. Chem. 284*, 21971−21980.

(36) Gakh, O., Bedekovics, T., Duncan, S. F., Smith, D. Y. t., Berkholz, D. S., and Isaya, G. (2010) Normal and Friedreich ataxia cells express different isoforms of frataxin with complementary roles in iron-sulfur cluster assembly. *J. Biol. Chem. 285*, 38486−38501.

(37) Yoon, T., and Cowan, J. A. (2003) Iron-sulfur cluster biosynthesis. Characterization of frataxin as an iron donor for assembly of [2Fe-2S] clusters in ISU-type proteins. *J. Am. Chem. Soc. 125*, 6078−6084.

(38) Pearson, R. G. (1968) Hard and Soft Acids and Bases HSAB 1. Fundamental Principles. *J. Chem. Educ. 45*, 581−.

(39) Asuru, A. P., and Busenlehner, L. S. (2011) Analysis of human ferrochelatase iron binding via amide hydrogen/deuterium exchange mass spectrometry. *Intl. J. Mass Spectrom. 302*, 76−84.

(40) Cavadini, P., Adamec, J., Taroni, F., Gakh, O., and Isaya, G. (2000) Two-step processing of human frataxin by mitochondrial

processing peptidase. Precursor and intermediate forms are cleaved at different rates. *J. Biol. Chem. 275*, 41469−41475.
(41) Yoon, T., Dizin, E., and Cowan, J. A. (2007) N-terminal iron-mediated self-cleavage of human frataxin: regulation of iron binding and complex formation with target proteins. *J. Biol. Inorg. Chem. 12*, 535−542.
(42) Dhe-Paganon, S., Shigeta, R., Chi, Y. I., Ristow, M., and Shoelson, S. E. (2000) Crystal structure of human frataxin. *J. Biol. Chem. 275*, 30753−30756.
(43) Larkin, M. A., Blackshields, G., Brown, N. P., Chenna, R., McGettigan, P. A., McWilliam, H., Valentin, F., Wallace, I. M., Wilm, A., Lopez, R., Thompson, J. D., Gibson, T. J., and Higgins, D. G. (2007) Clustal W and Clustal X version 2.0. *Bioinformatics 23*, 2947−2948.